JACS
JOURNAL OF THE AMERICAN CHEMICAL SOCIETY
Article
pubs.acs.org/JACS

Structural Evolution of Iron Antimonides from Amorphous Precursors to Crystalline Products Studied by Total Scattering Techniques

Sage R. Bauers,[†] Suzannah R. Wood,[†] Kirsten M. Ø. Jensen,[§] Anders B. Blichfeld,[‡] Bo B. Iversen,[‡] Simon J. L. Billinge,[§,⊥] and David C. Johnson*[,†]

[†]Department of Chemistry and Materials Science Institute, University of Oregon, Eugene, Oregon 97403, United States
[§]Department of Applied Physics and Applied Mathematics, Columbia University, New York, New York 10027, United States
[‡]Center for Materials Crystallography, Department of Chemistry and iNANO, Aarhus University, DK-8000 Aarhus C, Denmark
[⊥]Condensed Matter Physics and Materials Science Department, Brookhaven National Laboratory, Upton, New York 11973, United States

Supporting Information

ABSTRACT: Homogeneous reaction precursors may be used to form several solid-state compounds inaccessible by traditional synthetic routes, but there has been little development of techniques that allow for a priori prediction of what may crystallize in a given material system. Here, the local structures of $FeSb_x$ designed precursors are determined and compared with the structural motifs of their crystalline products. X-ray total scattering and atomic pair distribution function (PDF) analysis are used to show that precursors that first nucleate a metastable $FeSb_3$ compound share similar local structure to the product. Interestingly, precursors that directly crystallize to thermodynamically stable $FeSb_2$ products also contain local structural motifs of the metastable phase, despite their compositional disagreement. While both crystalline phases consist of distorted $FeSb_6$ octahedra with Sb shared between either two or three octahedra as required for stoichiometry, a corner-sharing arrangement indicative of AX_3-type structures is the only motif apparent in the PDF of either precursor. Prior speculation was that local composition controlled which compounds nucleate from amorphous intermediates, with different compositions favoring different local arrangements and hence different products. This data suggests that local environments in these amorphous intermediates may not be very sensitive to overall composition. This can provide insight into potential metastable phases which may form in a material system, even with a precursor that does not crystallize to the kinetically stabilized product. Determination of local structure in homogeneous amorphous reaction intermediates from techniques such as PDF can be a valuable asset in the development of systematic methods to prepare targeted solid-state compounds from designed precursors.

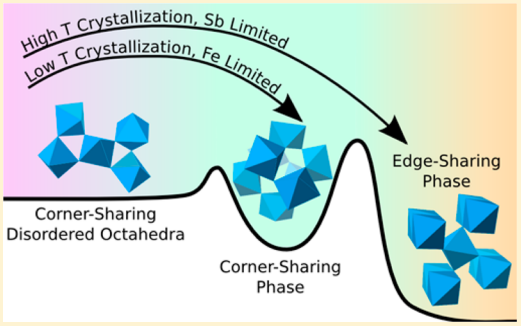

INTRODUCTION

Traditional solid-state synthesis requires high heat and long reaction times to drive the formation of a thermodynamic product.[1] During this process, atoms must diffuse over long distances, which is typically rather slow in solids and even on solid surfaces. Due to the concentration gradient at the reacting interfaces, a rich combination of compounds forms as interdiffusion, nucleation, and growth occur.[2] However, the elevated temperature and long reaction times ultimately limit the product to the thermodynamically stable mix of compounds at the temperature and composition of reaction. Moreover, the intermediate products and structural changes during the diffusion and crystallization process are difficult to follow. A general lack of a mechanistic understanding or even a description of the evolving structure during the formation of these compounds, as well as commercial interest in the functionality of inorganic materials, has moved solid-state synthesis from the realm of chemistry toward the domain of materials science.[3]

While many predictions of novel materials can be made, unlike the synthesis of organic compounds, there is currently no clear-cut path to direct the formation of specific metastable inorganic products from reactants. Various guidelines, such as Ostwald's step rule that states crystallization from a solution proceeds stepwise through increasingly favorable intermediates, may be applied to inorganic and solid systems, but use of them tends to be retrospective as opposed to predictive.[4] Recently, however, in situ monitoring of inorganic reactions has shown the formation of many metastable intermediate products as well as promising and controllable methods to synthesize them. For example, a clever in situ diffraction experiment recently

Received: May 9, 2015
Published: July 10, 2015

DOI: 10.1021/jacs.5b04838
J. Am. Chem. Soc. 2015, 137, 9652−9658

identified and isolated several new ternary sulfide phases in otherwise ordinary inorganic flux reactions.[5] Our knowledge of how inorganic reactions proceed has also been enhanced by X-ray total scattering studies of local structure during the formation of inorganic frameworks. Recent work on nanoparticle formation under hydrothermal conditions demonstrates the insights obtained from these studies.[6] The topic of in situ studies of the structural evolution of inorganic compounds was recently reviewed.[7] For the most part these (and similar) reports are from systems where the chemistry, at least in part, is occurring outside the solid-state. However, recently there has been considerable interest in better understanding the formation of inorganic compounds during solid-state reaction, hopefully leading to a renaissance in the field from a chemist's perspective.[8−11]

A fruitful approach to the discovery of new solid-state materials has been in vapor depositing thin films that are compositionally controlled at an atomic level, allowing for constituents to react at modest temperatures without the need for long-range solid-state diffusion.[1,12−16] This approach has been utilized in the synthesis of several new binary and ternary compounds.[17−20] Furthermore, by depositing constituents in layers that are thin enough, compounds not readily synthesizable by conventional solid-state techniques are formed.[14] It was proposed that under heating only thin layers would completely interdiffuse prior to nucleation. The homogeneous compositional environment was hypothesized to prevent nucleation of thermodynamically stable phases, as the systems lack a compositional gradient and would thus need to disproportionate to nucleate a thermodynamic compound with a different composition.[21] In this case, the slow diffusion rates become a synthetic advantage and can be used to help control the formation of kinetic products.[22] Particularly exciting is the possibility of "designing precursors" to yield desired products by controlling the deposition process. To realize the full potential of this method, it is essential to be able to characterize in detail not only the reaction products but also the amorphous precursors and the reaction pathways to the resulting product.

Here we have applied the atomic pair distribution function (PDF) analysis of X-ray diffraction data to study the local structure of a series of precursors that yield distinct products in the $FeSb_x$ (x = 2, 3) chemical system. Surprisingly, we see evidence of atomic scale interdiffusion and local metal coordinations representative of the final metastable product even in precursors compositionally unfavorable for its nucleation. The approach of coupling careful local structural measurements on homogeneous amorphous reaction intermediates represents a powerful approach that has extensions to the designed synthesis of a broad range of solid-state chemical systems.

Structures in $FeSb_x$ Chemical System. The iron−antimony phase diagram contains only two thermodynamic compounds: an $Fe_{1+x}Sb$ phase in which excess Fe resides interstitially in an otherwise NiAs-type structure and an $FeSb_2$ marcasite-type phase.[23] The marcasite structure can be thought of as rutile with a larger rotation between distorted $FeSb_6$ octahedra: octahedra are corner-sharing in the a−b plane and edge-sharing as they are translated down the c-axis. This results in a loss of symmetry, a stabilizing anion dimer, and an orthorhombic unit cell. An $FeSb_3$ phase that is always thermodynamically unstable relative to $FeSb_2$ + Sb has also been synthesized using modulated thin-film precursors.[24] This compound adopts a skutterudite structure, which is related to the ReO_3 structure but with four anions along parallel edges of the unit cell displaced inward, creating a four-fold ring. This doubles the edge length along each direction of the unit cell, with one-fourth of the octants containing an open "cage". In each of these compounds Fe is octahedrally coordinated with differing connectivity between octahedra, as expected by the changes in stoichiometry. In $Fe_{1+x}Sb$ the octahedra share faces. In $FeSb_2$, each corner Sb of the octahedra is shared by three octahedra, which are rotated to create a short Sb−Sb bonding pair. In $FeSb_3$, two octahedra share each corner. Figure 1 shows

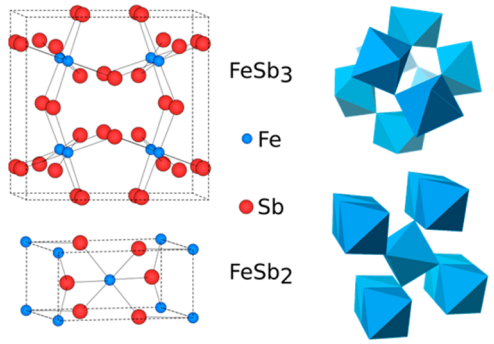

Figure 1. Crystalline phases of (top) $FeSb_3$ and (bottom) $FeSb_2$ in both ball-and-stick and polyhedral representations, generated from available crystallographic data.[24,30] The $FeSb_2$ polyhedral representation shows two unit-cells along each lattice vector (eight unit cells total). The $FeSb_3$ polyhedral representation has an offset origin relative to the ball-and-stick model.

representations of the structures of both $FeSb_2$ and $FeSb_3$. There has been much discussion on bonding within both the skutterudite and marcasite structural families. In each case, one could imagine a bonding scheme wherein formation of the $FeSb_6$ octahedral unit is the dominating interaction, followed by stabilization from dimerization ($FeSb_2$) or tetramerization ($FeSb_3$) of antimony. Similarly, the opposite case could reasonably occur, and historically much of the literature has centered around discussion of the Sb−Sb dimer and tetramer formation.[25−27] However, recent studies of both FeS_2 marcasites and $CoSb_3$ skutterudites show the metal octahedron plays a large role in the bonding.[28,29]

EXPERIMENTAL SECTION

Precursors were deposited using the modulated elemental reactants synthesis method on a custom-built deposition system.[31] Antimony was deposited from a Knudsen effusion cell, whereas an iron source was evaporated using an electron gun. A pressure below 5×10^{-7} Torr was maintained during deposition. Deposition rates were monitored from quartz crystal microbalances and shutters installed above each source were sequentially opened and closed to achieve a layered precursor of the desired thickness. Deposition parameters were calibrated to allow for targeted composition ratios and bilayer thicknesses between Fe and Sb. Samples used for calibrating the depositions had targeted total thicknesses of approximately 36 nm, whereas samples for further analysis had a targeted total thickness of approximately 360 nm. While calibrating the system, thicknesses were confirmed with X-ray reflectivity. Cumulative roughness combined with high-frequency Kiessig fringes prevented determining total thickness by this method on the thick films. The $FeSb_3$ samples were deposited with excess Sb as stoichiometric precursors (with 25 atomic % Fe) formed mixtures of the diantimonide and triantimonide phases as reported previously.[32]

DOI: 10.1021/jacs.5b04838
J. Am. Chem. Soc. 2015, 137, 9652−9658

The precursors discussed herein were deposited on adjacent substrates: polished (100) Si wafers and (100) Si wafers coated in poly(methyl methacrylate) (PMMA). Films on PMMA were then floated off of the support wafer by dissolving in acetone, washed to remove excess PMMA, and collected on a Teflon filter. This resulted in delicate flat metallic flakes with an approximate maximum diameter of 0.5 mm, which were removed from the filter and packed into a 1.0 mm kapton capillary. PDF data were taken on samples in three states: as-deposited with no high-temperature treatment, interdiffused wherein precursors are kept at 100 °C for 30 min in order to drive diffusion of the layers, and annealed in which precursors are held at a temperature that activates crystallization of the desired phase for 30 min. $FeSb_3$ samples were crystallized at 200 °C and $FeSb_2$ samples at 300 °C. All sample annealing was done on a hot plate in a nitrogen atmosphere after transfer to capillaries. No differences in capillary tubes were observed after thermal treatment.

Composition was measured from samples on bare Si using an electron probe microanalysis technique where the *k*-ratios are collected as a function of accelerating voltage.[33] Diffraction data for Rietveld refinement were collected from the samples deposited on bare polished Si using a Rigaku Smartlab diffractometer in grazing-incidence geometry and Cu−Kα radiation. Rietveld refinements were done using the GSAS[34] software package and EXPGUI[35] interface.

Room-temperature X-ray total scattering data were collected at a wavelength of 0.185970 Å at beamline X17A of the National Synchrotron Light Source, Brookhaven National Laboratory, from samples in filled kapton capillaries. The RA-PDF setup was used, with a PerkinElmer amorphous silicon detector.[36] The total scattering data were integrated using Fit2D,[37] and PDFs were generated with PDFgetX3[38] using a Q_{min} of 0.85 Å^{-1}, Q_{max} of 25 Å^{-1}, and an r_{poly} of 0.9. Real-space modeling of crystalline phases was done in PDFgui.[39]

RESULTS AND DISCUSSION

Following previous reports, we were able to design precursors such that they nucleate either the $FeSb_2$ or $FeSb_3$ phase.[32] Both precursors contained partially interdiffused elemental layers of Sb and Fe with thicknesses below the critical thickness for nucleation of the triantimonide. Thus, selectivity was achieved by adjusting elemental composition. Sb layer thickness was kept nearly constant between precursors. Table 1 summarizes the samples used in the PDF investigation.

Table 1. Summary of Precursors

phase	Fe th. (Å)	Sb th. (Å)	repeats	Fe/Sb
$FeSb_2$	2.4	16.8	188	0.49
$FeSb_3$	1.1	17.0	200	0.21

Figure 2 shows powder X-ray diffraction data from annealed thin-films of each sample and associated Rietveld refinements, which confirm the formation of the expected $FeSb_2$ and $FeSb_3$ phases. On annealing, the $FeSb_3$ samples remained as smooth films, whereas the $FeSb_2$ sample forms visible crystallites on the surface. Diffraction data collected at several incidence angles and in the plane of the film indicate scattering from powder-like samples. The diffraction data from the $FeSb_2$ sample contain a small Sb signal (as seen from, e.g., the Sb (012) peak at 2 Å^{-1}), though inclusion of Sb does not appreciably improve refinements. The $FeSb_3$ sample shows 34% Sb impurity by mass.

Figure 3 shows a portion of the PDFs from crystalline samples, along with their least-squares fits (*r*-range fit from 5 to 60 Å). Also shown are theoretical PDFs of the constituent phases, which were generated with lattice parameters obtained from the refined diffraction data shown in Figure 2. For the

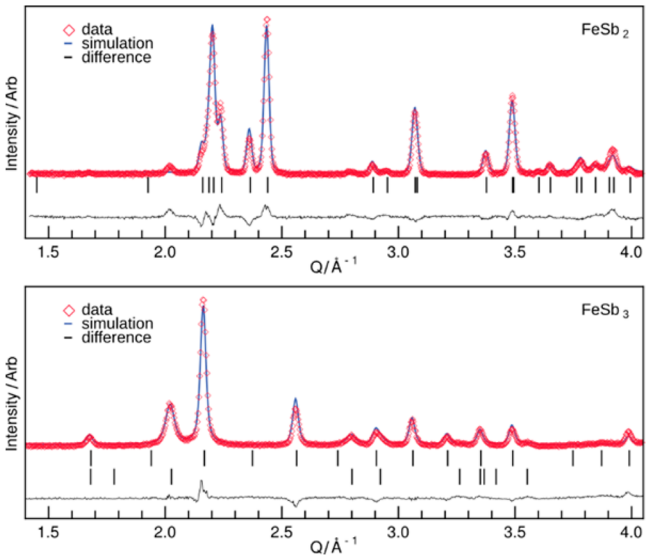

Figure 2. Diffraction patterns taken from iron antimonide samples. In the triantimonide phase, the above markers correspond to the marked phase, and the lower markers correspond to antimony. The markers in the diantimode pane refer to the marked phase.

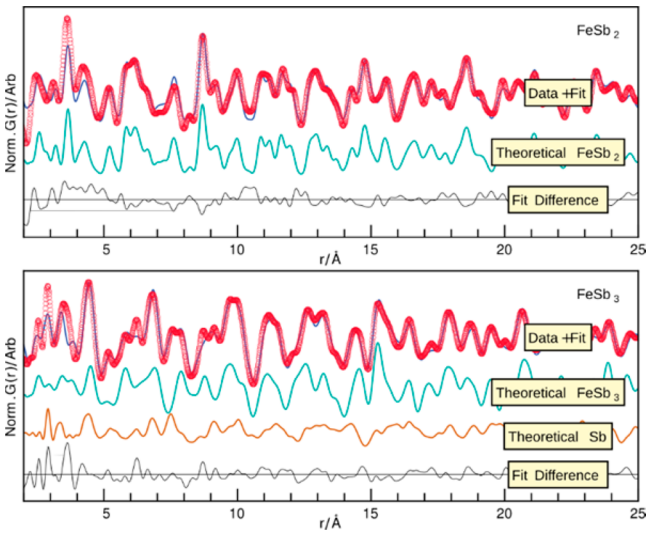

Figure 3. PDFs of $FeSb_2$ and $FeSb_3$ compounds with models as well as theoretical PDFs of constituent phases. The difference between data and fit is shown below in black. Fits were performed with an *r* range of 5−60 Å. For the full fit-range of the PDFs see the Supporting Information.

metastable sample, a two-phase fit including Sb and $FeSb_3$ was used. The $FeSb_2$ sample was fit with a single $FeSb_2$ phase as the addition of Sb to the model resulted in no practical improvement. In both cases, fits were done preserving cell symmetry with the fitted parameters being lattice parameters, scaling, correlated motion, particle diameter, and isotropic Debye−Waller factors. The correlated motion parameters were constrained to match between phases. The difference curve shows the model does not completely capture the short-range (r < 5 Å) order, with agreement improving at higher *r*. The $FeSb_3$ mass percentage relative to Sb from PDF refinement is slightly lower than from Rietveld refinement but probably within the limit of the error, 62% (PDF) vs 66% (Rietveld). Examination of the difference curve shows the strongest

DOI: 10.1021/jacs.5b04838
J. Am. Chem. Soc. 2015, 137, 9652−9658

Table 2. Summary of Pair Distances That Correspond to the First Peaks in the $FeSb_2$ and $FeSb_3$ PDFs

$FeSb_2$ pair distances			$FeSb_3$ pair distances		
Position / Å	Description	Schematic	Position / Å	Description	Schematic
2.6	Fe-Sb within $FeSb_6$ octahedra		2.6	Fe-Sb within $FeSb_6$ octahedra	
2.9	Sb-Sb dimers between corner sharing octahedra		2.9	Sb-Sb in Sb metal and Sb tetramers between $FeSb_6$ octahedra	
3.2	Fe-Fe, Sb-Sb along translation direction of edge-sharing octahedra		3.3-3.5	Sb-Sb along short octahedral edges	
3.6-3.7	Sb-Sb along medium octahedral edges		3.8	Sb-Sb along long octahedral edges	
4.1-4.4	Various inter-octahedral Fe-Sb and Sb-Sb along longest octahedral edges		4.5-4.6	Various pairs (Fe-Fe, Fe-Sb, Sb-Sb) between octahedra	
5.2	Sb-Sb along opposite corners of $FeSb_6$ octahedra		5.1	Sb-Sb along opposite corners of $FeSb_6$ octahedra	

disagreement at ca. 2.9 Å. This corresponds to the nearest Sb pair distance in bulk Sb and indicates the misfit at low *r*-values is likely due to the presence of additional amorphous Sb that is not included in the model of crystalline Sb and $FeSb_3$. Any additional disagreement at low *r* may be due to remaining amorphous material or artifacts from data reduction. The results from the PDF refinements regarding the crystalline phases agree well with the structural models determined from prior results based on powder X-ray diffraction analysis. Interestingly, our data suggest that in this system the densities do not evolve according to the Ostwald rule. In fact, the refinement of the $FeSb_3$ sample shows a slightly higher density than for the marcasite structure. Further details of these refinements are provided in the Supporting Information.

Table 2 summarizes the pairs seen in the PDFs of each crystalline phase up to about 5 Å. This *r*-range contains all intraoctahedral distances as well as the first few interoctahedral pairs. The schematic showing pair distances denotes Fe in carmine and Sb in cyan. Both PDFs contain sharp peaks in the lowest *r*-range, while broader peaks are seen at ca. 3.5 and 4.4 Å from multiple pairs in close proximity around these distances. There is a ∼1 Å difference in Sb−Sb pair distances along the various $FeSb_6$ octahedral edges in $FeSb_2$. The shortest and longest pair distances belong to the translated and shared edges, respectively. Multiple electronic arguments have been previously proposed to account for the structural distortion of the metal octahedra in marcasites.[40,41]

In previous work, Williams et al. attributed an exotherm at 140 °C in precursor films to the crystallization of $FeSb_3$, while an exothermic signal before the nucleation event has been associated with interdiffusion of the elemental layers.[32] Diffraction data from as-deposited and interdiffused (heat treated at 100 °C in a nitrogen environment for 30 min to drive solid-state diffusion of the layers) samples show an order of magnitude decrease in intensity from the (001) superlattice reflection, indicating significant intermixing has occurred, though some modulation in electron density remains (see Supporting Information). To follow structural changes as the samples evolve from the as-deposited state to the final annealed phases, X-ray total scattering data were collected on powders in the as-deposited, interdiffused, and annealed states. The total scattering data were used to generate PDFs, which are shown in Figure 4 for both the $FeSb_2$ and $FeSb_3$ compounds. For both

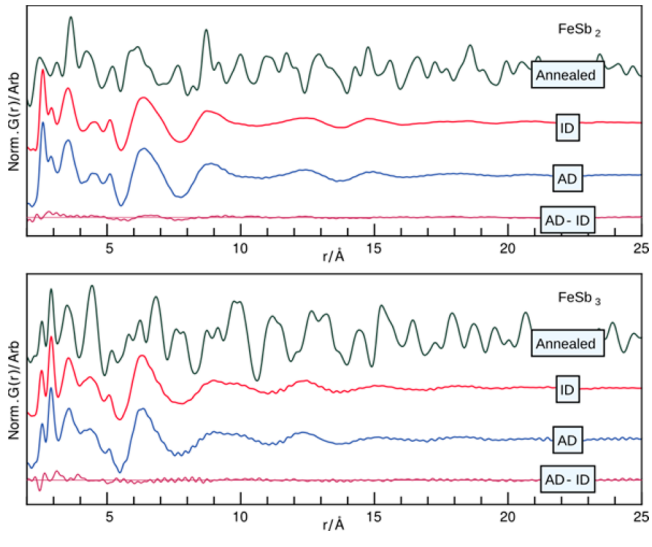

Figure 4. Pair distribution functions of as-deposited (AD), interdiffused (ID), and annealed samples generated from total scattering data. The difference curves between the as-deposited and interdiffused samples (AD−ID) show little structural change during the diffusion process, as seen by the small deviations from the lines showing zero change.

the as-deposited and interdiffused samples, only short-range order is seen, while long-range order from crystalline compounds is only seen in the annealed samples. Interestingly, the PDFs obtained on the as-deposited and interdiffused samples are very similar, as shown by the difference curves. This implies that the local structure of both the $FeSb_3$ and $FeSb_2$ precursors does not change significantly during the initial heating of the samples and that significant interdiffusion

DOI: 10.1021/jacs.5b04838
J. Am. Chem. Soc. 2015, 137, 9652−9658

between the Fe and Sb layers happens during deposition, at room temperature, or during the removal of the films from the substrate. For all four amorphous samples, a series of sharp peaks are seen at the lowest *r*-values, showing well-ordered local structures. The distance at which a highly ordered structure terminates is consistent between both the $FeSb_2$ and $FeSb_3$ precursors with the last high-frequency peak at ca. 5.1 Å followed by an intense, broad signal centered at 6.4 Å and regular oscillations to higher *r*. The domain size for midrange order is given by these oscillations and appears very similar between the two precursors. The pair distances and *r*-value where sharp peaks disappear in the amorphous $FeSb_3$ samples correspond well to the residuals in the fit of the crystalline $FeSb_3$ sample (Figure 3), indicating that some amorphous $FeSb_6$ octahedra remain. No similar correlations with the residuals of the $FeSb_2$ residuals could be made. Cursory examinations of the PDFs show that the local structure in the two precursors are different from one another, as might be expected from the difference in average composition.

Panels a and b of Figure 5 show PDFs of the crystalline samples overlaid with their as-deposited amorphous precursors,

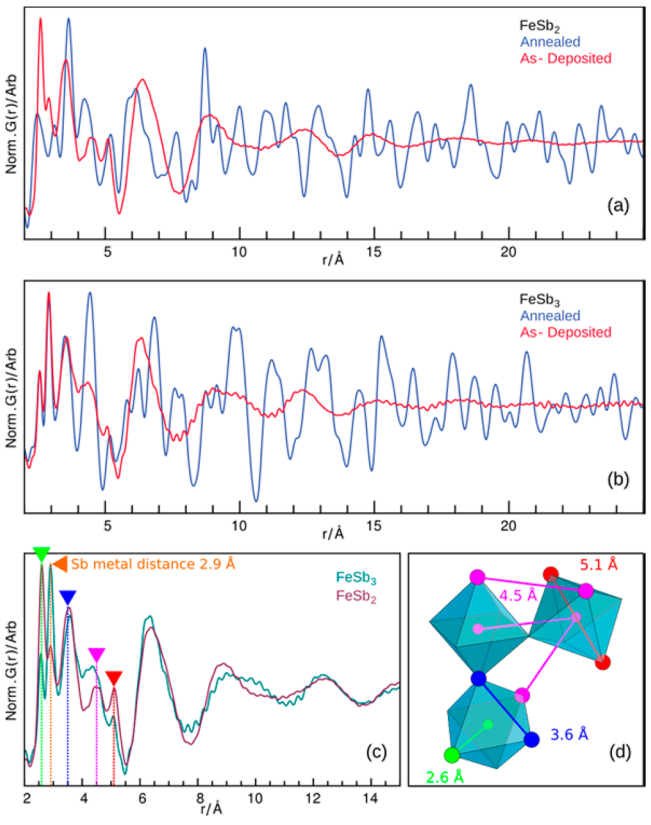

Figure 5. PDFs of precursors overlaid with annealed samples for (a) $FeSb_2$ and (b) $FeSb_3$. (c) Overlaid $FeSb_2$ and $FeSb_3$ precursors show similar peak positions but varying relative intensities. Peak positions corresponding to pairs in the $FeSb_3$ PDF are shown by colored triangles. (d) Similar pair distances from a disordered arrangement of corner sharing octahedra are shown in corresponding colors.

with each curve normalized to its maximum intensity. The $FeSb_3$ data show large similarities between amorphous and crystalline PDFs in the local structure. Up to about 5 Å, vestiges of the $FeSb_3$ product can be seen, with contributions from excess Sb also clearly manifested by a sharp narrow peak at 2.9 Å. This suggests the presence of amorphous Sb with only very short-range order as well as corner sharing $FeSb_6$ octahedra without the regular orientation found in the crystalline structure. By comparing to the atomic pairs giving rise to PDF peaks from the crystalline phases (summarized in Table 2), the structural motifs in the amorphous samples can be identified, as illustrated in Figure 5c. The relative intensities of peaks from Sb pairs within an octahedron (3.5 Å for pairs along an edge and 5.1 Å through the center, indicated in Figure 5 by blue and red, respectively) are approximately the same between as-deposited and annealed $FeSb_3$ samples. However, the pair intensity around 4.5 Å, which corresponds to multiple pairs across octahedra in the crystalline structure, is broad and low in the amorphous PDF due to the large number of interoctahedral distances which may occur between disordered corner-sharing octahedra (Figure 5d, shown in magenta). Notably, no vestiges of edge-sharing octahedra, which produces multiple pairs at 3.2 Å as seen in the crystalline $FeSb_2$ sample (see Table 2), are apparent in the $FeSb_3$ precursor. The similarity between the $FeSb_3$ precursor and product helps explain the low nucleation temperature. The data suggest that reorientation of existing corner-sharing octahedra into a regular extended network is the predominant mechanism of crystallization on heating.

Conversely, Figure 5a shows that the PDF of the precursor that nucleates to $FeSb_2$ does not match the crystalline phase well, even at low *r*. In fact, while relative intensities differ, the local structure only shows motifs of corner-sharing Fe−Sb octahedra similar to the $FeSb_3$ phase and precursor. This is clear in Figure 5c, where the PDFs from the two precursors are overlaid. Comparing precursors, a large increase in the relative amplitude of the 2.6 Å peak corresponding to the Fe−Sb distance (in $FeSb_6$ octahedra) is apparent and attributable to the increased iron content in the sample. The 3.2 Å pair distance, which corresponds to adjacent edge-sharing octahedra translated along the *c*-direction in $FeSb_2$, is not observed in the as-deposited PDFs. If the marcasite edge-sharing motif were present in the $FeSb_2$ precursor, additional intensity manifested as a narrow peak would be expected at this pair distance, due to every atom having an interoctahedral pair along the translation direction. This is observed in the crystalline $FeSb_2$ PDF, but from the lack of this feature in the precursor we conclude edge sharing is absent. Without edge-sharing, the $FeSb_2$ sample does not have enough antimony to fully coordinate each iron octahedrally. However, the similarities in the as-deposited precursor and interdiffused precursor PDFs suggest that Fe in $FeSb_3$ and Sb in $FeSb_2$ are completely coordinated on deposition. With this in mind, the presence of a small signal at the characteristic 2.9 Å Sb−Sb pair distance in the $FeSb_2$ precursor is at first puzzling. However, this pair distance is explained by interoctahedral Sb dimers. Notably, both the $FeSb_2$ and $FeSb_3$ precursors exhibit an inherent stability in the $FeSb_6$ structural unit. Unlike the $FeSb_3$ sample in which existing building blocks primarily need to arrange themselves into a regular structure, extra iron must be incorporated into the edge-sharing marcasite structure of $FeSb_2$. The large differences between the precursor and product help explain the higher energy required to nucleate the $FeSb_2$ phase relative to $FeSb_3$.

Previous investigations have suggested that nucleation of metastable products from well-mixed precursors is driven by forcing a local environment of similar structure and composition to the kinetic phase. Somewhat surprisingly, the results summarized in Figure 5 indicate that even without the excess Sb, the local structure of the $FeSb_2$ precursor is more similar to $FeSb_3$. It then appears that in these systems there is

DOI: 10.1021/jacs.5b04838
J. Am. Chem. Soc. 2015, 137, 9652−9658

an inherent kinetic favorability toward adopting a structure similar to the metastable phase, which can then be nucleated in precursors with appropriate composition. The idea that similarity in the local structure of a precursor to the phase that it nucleates is something we may be able to extend to other metastable solid-state compounds and suggests in general that homogeneous amorphous intermediates might be very useful synthetic tools. Probing local structure of reaction intermediates using PDF might allow for rational changes to be made in composition to avoid local structure similar to known compounds and/or to tune composition of the amorphous precursor to obtain local structures similar to targeted compounds to promote nucleation. The observation of the same structures in both as-deposited and interdiffused states illustrates the stability of the corner-sharing $FeSb_6$ structural motif. If this approach proves to be general for the formation of metastable structures from amorphous reaction intermediates, it will be especially valuable when combined with ab initio calculation of stable local structures.

CONCLUSIONS

Local structural similarities of homogeneous amorphous iron and antimony precursors to a skutterudite crystal help to nucleate a low-temperature metastable $FeSb_3$ phase. Significant interdiffusion of the precursors, which are deposited in layers on the Å scale, occurs even at room temperature, leading to a nucleation-limited crystallization event. On deposition, constituents form an amorphous network of corner-sharing $FeSb_6$ octahedra similar to AX_3 structures, even in precursors with a 1:2 Fe:Sb ratio. This indicates preferential low-temperature formation toward the metastable phase is somewhat contrary to previous reports, where it was surmised the excess Sb drove the reaction toward the metastable product. The higher temperatures necessary for the crystallization of the thermodynamic $FeSb_2$ phase are most likely due to a major reorientation of local environment. In further studies it will be insightful to investigate this further and see at which point compositional disagreement overcomes the observed preference to form the corner-sharing $FeSb_6$ octahedra.

Continued use of PDF analysis in solid-state systems nucleated from homogeneous amorphous precursors will provide insightful information correlating precursor structures with final products. This will be particularly helpful in systems where many phases could form or systems wherein ternary or quaternary phases form instead of binary phases. Ultimately, similar analysis could be potentially used as a screening mechanism to optimize a precursor to have local structure similar to a predicted but unrealized compound. Given the appropriate synthetic control, a range of structural and compositional "designed precursors" could be formed, and their local structures tested for motifs of a targeted phase. This would provide valuable insight, greatly enhance the likelihood of synthetic success, and reduce the number of required experiments when exploring additional unknowns.

ASSOCIATED CONTENT

Supporting Information

Detail regarding PDF and Rietveld refinements. The Supporting Information is available free of charge on the ACS Publications website at DOI: 10.1021/jacs.5b04838.

AUTHOR INFORMATION

Corresponding Author

*davej@uoregon.edu

Notes

The authors declare no competing financial interest.

ACKNOWLEDGMENTS

The authors acknowledge support from the National Science Foundation under grant DMR-1266217. S.B. and S.W. were supported by the National Science Foundation through CCI grant no. CHE-1102637. B.B.I. was supported in part by the Danish National Research Foundation (Center for Materials Crystallography, DNRF93). A.B. would like to acknowledge the Sino-Danish Center for funding. K.J. is grateful for funding from the Villum Foundation, and work in the Billinge group was supported by U.S. Department of Energy, Office of Science, Office of Basic Energy Sciences (DOE-BES) under contract DE-SC00112704. The authors thank Milinda Abeykoon for assistance at Beamline X17A at the National Synchrotron Light Source, Brookhaven National Laboratory. Use of the National Synchrotron Light Source, Brookhaven National Laboratory, was supported by the DOE-BES, under contract no. DE-AC02-98CH10886.

REFERENCES

(1) Stein, A.; Keller, S. W.; Mallouk, T. E. *Science* **1993**, *259*, 1558−1564.
(2) West, A. R. *Solid State Chemistry and Its Applications*; John Wiley & Sons: Hoboken, NJ, 2007.
(3) DiSalvo, F. J. *Science* **1990**, *247*, 649−655.
(4) Chung, S.-Y.; Kim, Y.-M.; Kim, J.-G.; Kim, Y.-J. *Nat. Phys.* **2009**, *5*, 68−73.
(5) Shoemaker, D. P.; Hu, Y.-J.; Chung, D. Y.; Halder, G. J.; Chupas, P. J.; Soderholm, L.; Mitchell, J. F.; Kanatzidis, M. G. *Proc. Natl. Acad. Sci. U. S. A.* **2014**, *111*, 10922−10927.
(6) Jensen, K. M. Ø.; Christensen, M.; Juhas, P.; Tyrsted, C.; Bøjesen, E. D.; Lock, N.; Billinge, S. J. L.; Iversen, B. B. *J. Am. Chem. Soc.* **2012**, *134*, 6785−6792.
(7) Pienack, N.; Bensch, W. *Angew. Chem., Int. Ed.* **2011**, *50*, 2014−2034.
(8) Chen, Z.; Ren, Y.; Qin, Y.; Wu, H.; Ma, S.; Ren, J.; He, X.; Sun, Y.-K.; Amine, K. *J. Mater. Chem.* **2011**, *21*, 5604.
(9) Lebreton, F.; Belin, R. C.; Prieur, D.; Delahaye, T.; Blanchart, P. *Inorg. Chem.* **2012**, *51*, 9369−9375.
(10) Sarkar, S.; Peter, S. C. *Inorg. Chem.* **2013**, *52*, 9741−9748.
(11) Martinolich, A. J.; Neilson, J. R. *J. Am. Chem. Soc.* **2014**, *136*, 15654−15659.
(12) Johnson, D. C. *Curr. Opin. Solid State Mater. Sci.* **1998**, *3*, 159−167.
(13) Behrens, M.; Kiebach, R.; Bensch, W.; Häussler, D.; Jäger, W. *Inorg. Chem.* **2006**, *45*, 2704−2712.
(14) Fukuto, M.; Hornbostel, M. D.; Johnson, D. C. *J. Am. Chem. Soc.* **1994**, *116*, 9136−9140.
(15) Fischer, D.; Jansen, M. *J. Am. Chem. Soc.* **2002**, *124* (14), 3488−3489.
(16) Bach, A.; Fischer, D.; Jansen, M. *Z. Anorg. Allg. Chem.* **2013**, *639* (3-4), 465−467.
(17) Smalley, A. L. E.; Jespersen, M. L.; Johnson, D. C. *Inorg. Chem.* **2004**, *43*, 2486−2490.
(18) Berseth, P. A.; Hughes, T. A.; Schneidmiller, R.; Smalley, A.; Johnson, D. C. *Solid State Sci.* **2002**, *4*, 717−722.
(19) Regus, M.; Kuhn, G.; Polesya, S.; Mankovsky, S.; Alemayehu, M.; Stolt, M.; Johnson, D. C.; Ebert, H.; Bensch, W. *Z. Kristallogr. - Cryst. Mater.* **2014**, *229*, 229.
(20) Bach, A.; Fischer, D.; Mu, X.; Sigle, W.; van Aken, P. A.; Jansen, M. *Inorg. Chem.* **2011**, *50* (4), 1563−1569.

DOI: 10.1021/jacs.5b04838
J. Am. Chem. Soc. 2015, 137, 9652−9658

(21) Fister, L.; Novet, T.; Grant, C. A.; Johnson, D. C. *ChemInform* **1994**, *25*, 25.
(22) Anderson, M. D.; Thompson, J. O.; Johnson, D. C. *Chem. Mater.* **2013**, *25*, 3996−4002.
(23) Richter, K. W.; Ipser, H. *J. Alloys Compd.* **1997**, *247*, 247−249.
(24) Hornbostel, M. D.; Hyer, E. J.; Thiel, J.; Johnson, D. C. *J. Am. Chem. Soc.* **1997**, *119*, 2665−2668.
(25) Goodenough, J. B. *J. Solid State Chem.* **1972**, *5*, 144−152.
(26) A Papoian, G.; Hoffmann, R. *Angew. Chem., Int. Ed.* **2000**, *39*, 2408−2448.
(27) Jung, D.; Whangbo, M. H.; Alvarez, S. *Inorg. Chem.* **1990**, *29*, 2252−2255.
(28) Schmøkel, M. S.; Bjerg, L.; Cenedese, S.; Jørgensen, M. R. V.; Chen, Y.-S.; Overgaard, J.; Iversen, B. B. *Chem. Sci.* **2014**, *5*, 1408.
(29) Schmøkel, M. S.; Bjerg, L.; Overgaard, J.; Larsen, F. K.; Madsen, G. K. H.; Sugimoto, K.; Takata, M.; Iversen, B. B. *Angew. Chem., Int. Ed.* **2013**, *52*, 1503−1506.
(30) Holseth, H.; Kjekshus, A. *Acta Chem. Scand.* **1969**, *23*, 3043−3050.
(31) Noh, M.; Johnson, C. D.; Hornbostel, M. D.; Thiel, J.; Johnson, D. C. *Chem. Mater.* **1996**, *8*, 1625−1635.
(32) Williams, J. R.; Johnson, M.; Johnson, D. C. *J. Am. Chem. Soc.* **2001**, *123*, 1645−1649.
(33) Phung, T. M.; Jensen, J. M.; Johnson, D. C.; Donovan, J. J.; McBurnett, B. G. *X-Ray Spectrom.* **2008**, *37*, 608−614.
(34) Larson, A. C.; Von Dreele, R. B. *GSAS, General Structure Analysis System*; Los Alamos National Laboratory: Los Alamos, NM, 1994.
(35) Toby, B. H. *J. Appl. Crystallogr.* **2001**, *34*, 210−213.
(36) Chupas, P. J.; Qiu, X.; Hanson, J. C.; Lee, P. L.; Grey, C. P.; Billinge, S. J. L. *J. Appl. Crystallogr.* **2003**, *36*, 1342−1347.
(37) Hammersley, A. P.; Svensson, S. O.; Hanfland, M.; Fitch, A. N.; Hausermann, D. *High Pressure Res.* **1996**, *14*, 235−248.
(38) Juhas, P.; Davis, T.; Farrow, C. L.; Billinge, S. J. L. *J. Appl. Crystallogr.* **2013**, *46*, 560−566.
(39) Farrow, C. L.; Juhas, P.; Liu, J. W.; Bryndin, D.; Božin, E. S.; Bloch, J.; Proffen, T.; Billinge, S. J. L. *J. Phys.: Condens. Matter* **2007**, *19*, 335219.
(40) Hulliger, F.; Mooser, E. *J. Phys. Chem. Solids* **1965**, *26*, 429−433.
(41) Brostigen, G.; Kjekshus, A. *Acta Chem. Scand.* **1970**, *24*, 2983−2992.

DOI: 10.1021/jacs.5b04838
J. Am. Chem. Soc. 2015, 137, 9652−9658